Nuclear Import Pathway of the Telomere Elongation Supressor TRF1: Inhibition by Importin α

Jade K. Forwood and David A. Jans*

Nuclear Signaling Laboratory, Division for Biochemistry and Molecular Biology, John Curtin School of Medical Research, Canberra City, Australia, and Department for Biochemistry and Molecular Biology, Monash University, Clayton, Victoria 3152, Australia

Received January 14, 2002; Revised Manuscript Received May 26, 2002

ABSTRACT: Telomere repeat factor 1 (TRF1) regulates the steady-state length of chromosomes, whereby its overexpression results in telomere shortening while dominant negative TRF1 mutations can lead to telomere elongation, which is linked to cell immortalization/transformation. Although present in the nucleus at mammalian chromosomal ends during interphase and mitosis, nothing is known of the mechanism by which TRF1 enters the nucleus or how its nuclear levels may be regulated and the relevance of this, in turn, to telomere length and cell immortalization. Here we examine the nuclear import mechanism of TRF by expressing and purifying a recombinant TRF1−GFP (green fluorescent protein) fusion protein that is functional in terms of being able to bind telomeric DNA specifically as shown using a novel, quantitative double-label gel mobility shift assay. We quantitate the ability of TRF1−GFP to accumulate in the nucleus using real time confocal laser scanning microscopy, showing that the nuclear import pathway of TRF1 is mediated by importin (Imp) β1 and Ran. Impβ is shown to bind directly to TRF1 with nanomolar affinity using native gel electrophoretic and fluorescence polarization (FP) approaches; FP experiments also demonstrate that Impβ residues 1−380 are responsible for TRF1 binding. Intriguingly, when dimerized to Impβ, Impα was found to inhibit Impβ-mediated nuclear accumulation, although not affecting Impβ binding to TRF1. The study represents the first elucidation of the nuclear transport mechanism of TRF1; that its nuclear import is mediated directly by Impβ but inhibited by Impα may represent a novel regulatory mechanism, with potential relevance to oncogenesis.

Telomeres are protective caps at the end of chromosomes that ensure that chromosome length is maintained during replication, aberrant telomere length leading to cell immortalization/transformation and/or senescence/death (*1*, *2*). Telomeres are composed of telomeric DNA (G-rich DNA repeats) complexed with proteins, one of which is telomere repeat factor 1 (TRF1) (TTAGGG-repeat binding factor) (*3*−*5*). Recent evidence suggests that TRF1 has a role in suppressing the activity of telomerase, the enzyme responsible for the extension of the G-rich strand to form telomeric DNA (*1*). Increased telomere length has been linked directly to cancer, so that it is of great significance that overexpression of TRF1 in a human fibrosarcoma cell line HTC75 leads to a reduction of telomere length at a rate of 10 bp/cell division while expression of a dominant negative allele of TRF1 results in telomere elongation (*2*). Although TRF1 is clearly nuclear, being bound to telomeres during interphase and mitosis (*5*), the mechanism by which it enters the nucleus has not been investigated; clearly, its nuclear levels are critical in determining telomere length and ultimately cell immortalization (*2*, *4*).

Proteins such as TRF1 that function in the nucleus gain nuclear access through the action of an intrinsic nuclear targeting signal (NTS) that is recognized by the cellular factors which mediate translocation of NTS-containing nuclear import substrates across the nuclear envelope (NE). In conventional nuclear protein import, the NTS is recognized by a heterodimeric complex of importin (Imp) subunits: Impα, which binds the NTS, and Impβ (Impβ1), which docks the transport complex at the NE-localized nuclear pore complex (NPC) through interaction with nucleoporins (*6*). The NTS substrate−Imp complex is then believed to be translocated through the NPC by a series of interactions with nucleoporins that line its central channel. Upon arrival at the nucleoplasmic side of the NPC, the NTS-containing substrate−Imp complex is dissociated in the nucleus through binding of the monomeric guanine nucleotide binding protein Ran in its GTP-bound form to Impβ (*7*). The nuclear protein is then free to perform its designated function, while Imps are recycled back to the cytoplasm for subsequent rounds of nuclear import (*8*).

In many cases, key cellular events can be regulated by controlling the access of specific proteins to their site of function such as transcription factor (TF) access to promoter sequences in the nucleus (*9*). In this context, it is becoming clear that the specific nuclear import pathway utilized by a TF or other nuclear protein is critical in determining how the protein's nuclear transport may be regulated (*10*). Many constitutively nuclear TFs, for example, appear to be transported to the nucleus through direct interaction with

* Correspondence should be addressed to this author at the Nuclear Signaling Laboratory, Department of Biochemistry and Molecular Biology, P.O. Box 13D, Monash University 3800, Australia. Telephone: 00613/99053778. Telefax: 00613/99054699. E-mail: David.Jans@med.monash.edu.au.

10.1021/bi025548s CCC: $22.00
Published on Web 06/26/2002

Impβ, while inducible TFs whose nuclear translocation is regulated by cellular signals are generally recognized by the Impα/β heterodimer, with the interaction specifically regulated by mechanisms such as phosphorylation or NTS masking (*9*). This must be understood in the cellular context of intense competition between nuclear import substrates and transport factors for efficient transport to the nucleus (*10*).

The mechanistic basis of TRF1 nuclear import has not been studied in terms of either the signal responsible for mediating nuclear translocation or the pathway through which it might occur. In this study we examine the nuclear import pathway of TRF1, monitoring its nuclear translocation in "real time" for the first time and describing a novel, double-labeled fluorescent native gel shift assay to examine DNA-binding properties in the presence of Imps. The results indicate that nuclear import of TRF1 is mediated by Impβ and Ran. Impα appears to inhibit Impβ-mediated nuclear accumulation, opening up the possibility that it may negatively regulate TRF1 nuclear entry. This may have implications for modulation of TRF1 nuclear levels and ultimately telomere length.

MATERIALS AND METHODS

Construction, Expression, and Purification of GFP−TRF1 Fusion Protein. A DNA fragment encoding the Myb-like DNA-binding domain of human TRF1 (*4*) together with the flanking putative NTS (TRF1 residues 337−441) was amplified by PCR to include terminal *Nhe*I restriction sites and cloned into the unique *Nhe*I site of the hexahistidine-tagged green fluorescent protein (GFP) fusion protein expression vector pTRCAHisGFPNheI (*11*). The fidelity of the construct was verified by DNA sequencing. Host strain M15 was grown at 28 °C until mid-log phase whereupon GFP−TRF1 was overexpressed by induction with 1 mM IPTG for 8 h. The bacteria were collected by centrifugation and resuspended in His buffer (50 mM phosphate buffer, pH 8, 10 mM Tris, pH 8, and 300 mM NaCl) containing 8 M urea. Cell debris was removed by centrifugation and the supernatant incubated with 2 mL of prewashed Ni-NTA−agarose (QIAGEN) for 2 h at 4 °C. The matrix was then washed extensively with His buffer/8 M urea containing 20 mM imidazole, and refolding of the still bound GFP−TRF1 was performed on the column by slow (2 h) stepwise dilution of His buffer lacking urea. GFP−TRF1 was then eluted from the column by incubation with His buffer containing 500 mM imidazole. The buffer was then exchanged with PBS using a PD-10 column (Pharmacia), and aliquots were stored at −70 °C.

In Vitro Nuclear Transport Assay and Kinetics. Nuclear import was analyzed at the single cell level using mechanically perforated HTC cells in conjunction with confocal laser scanning microscopy (CLSM) (*12*−*15*). Experiments were performed in a 5 μL volume containing transport substrate (1.0 μM GFP−TRF1), a control 70 kDa Texas Red labeled dextran (Molecular Probes) to assess nuclear integrity, BSA (45 mg/mL), and intracellular buffer (final concentration: 30 mM KCl, 1.2 mM $NaHCO_3$, 1.2 mM $MgCl_2$, 0.3 mM EGTA, 0.03 mM $CaCl_2$, and 24 mM HEPES). Where cytosol was used, BSA was replaced with untreated reticulocyte lysate (Promega) as previously described (*12*). The assay was monitored over 45 min at 1 min intervals and quantitative analysis of nuclear import kinetics performed as previously described (*12*−*15*) using the NIH Image software (*12*−*15*).

Expression and Purification of Imps. Mouse Impα (PTAC58) and Impβ (PTAC97) Imp subunits and human Ran were expressed in bacteria as glutathione *S*-transferase (GST) fusion proteins and purified as previously described (*12*−*16*). RanGST cleavage with thrombin and subsequent reconstitution with GDP or the nonhydrolyzable GTP analogue GTPγS were performed as previously described (*17*). Where used, the Impα/β complex was preformed at 13.6 μM (equimolar ratio) in the presence of 1 mM DTT as described previously (*12*−*16*); dimerization (K_d of 2.2 nM) (*14*) is complete under these conditions. The full-length and truncated forms of hexa-His-tagged human Impβ were expressed and purified by Ni-NTA chromatography as previously described (*17*), while the hexa-His-tagged RanBP5 (Impβ3) was similarly expressed and purified (*18*).

Gel Mobility Shift Assay. Probes containing specific DNA-binding recognition sequences (underlined) for TRF1 were prepared by annealing complementary oligonucleotides: TRF1 top, 5′ GATCGGTCGAC<u>TTAGGGTTAGGG</u>CATTATGATC 3′; bottom, 5′ GATCGATCATAATG<u>CCCTAACCCTAA</u>GTCGACC 3′. The double-stranded oligonucleotides were then purified by electrophoresis, and the concentration was estimated from absorbance measurements. Probes were end-labeled using the Texas Red dCTP−Texas Red labeling kit (Bio-Rad), and unincorporated dye was removed by ethanol precipitation. TRF1 binding to the probe was assessed by incubating 1 μM GFP−TRF1 with 0.1 μM labeled probe in binding buffer (10 mM Tris, 1 mM $MgCl_2$, 0.1% NP40, 10 mM DTT, 0.8 mM EDTA, 3% glycerol, and 1.5% sucrose) at room temperature for 15 min, before electrophoresis at 4 °C on a 5% native polyacrylamide gel. The gel was visualized on a Fuji Film FLA3000 gel imaging system for GFP (ex 473 nm; Y520 filter) and Texas Red (ex 532 nm; O580 filter), and the results were quantified using the ImageGauge software as previously described (*11*, *17*). Molar ratios of protein to DNA in particular bands were calculated by determining, after the subtraction of background, the fluorescence associated with each band relative to the comparable fluorescence value for the total protein or DNA loaded, respectively.

For mobility shift assays involving protein−protein interactions, 1 μM GFP−TRF1 was incubated with 3000−25 nM Imps for 20 min prior to electrophoresis as described above. Gels were directly analyzed on the Fuji Film FLA3000 for GFP (ex 473 nm; Y520 filter) and Texas Red (ex 532 nm; O580 filter) and quantified using the ImageGauge software. The bands reflecting GFP−TRF1 alone or in specific complexes with DNA were discerned from background for quantitation purposes by placing a square of constant area around each band. Backgrounds were handled by subtracting the autofluorescence of the gel measured in an identical area placed at the same position in an empty lane of the gel. Fluorescence resonance energy transfer from the emission of GFP (donor) to Texas Red (acceptor) is not a factor in this double-label analysis due to the negligible overlap of donor emission and the Texas Red excitation spectra with the specific excitation and emission filters (see above) used (*17*).

Fluorescence Polarization Assay. Fluorescence polarization (FP) was used to analyze GFP−TRF1−importin interac-

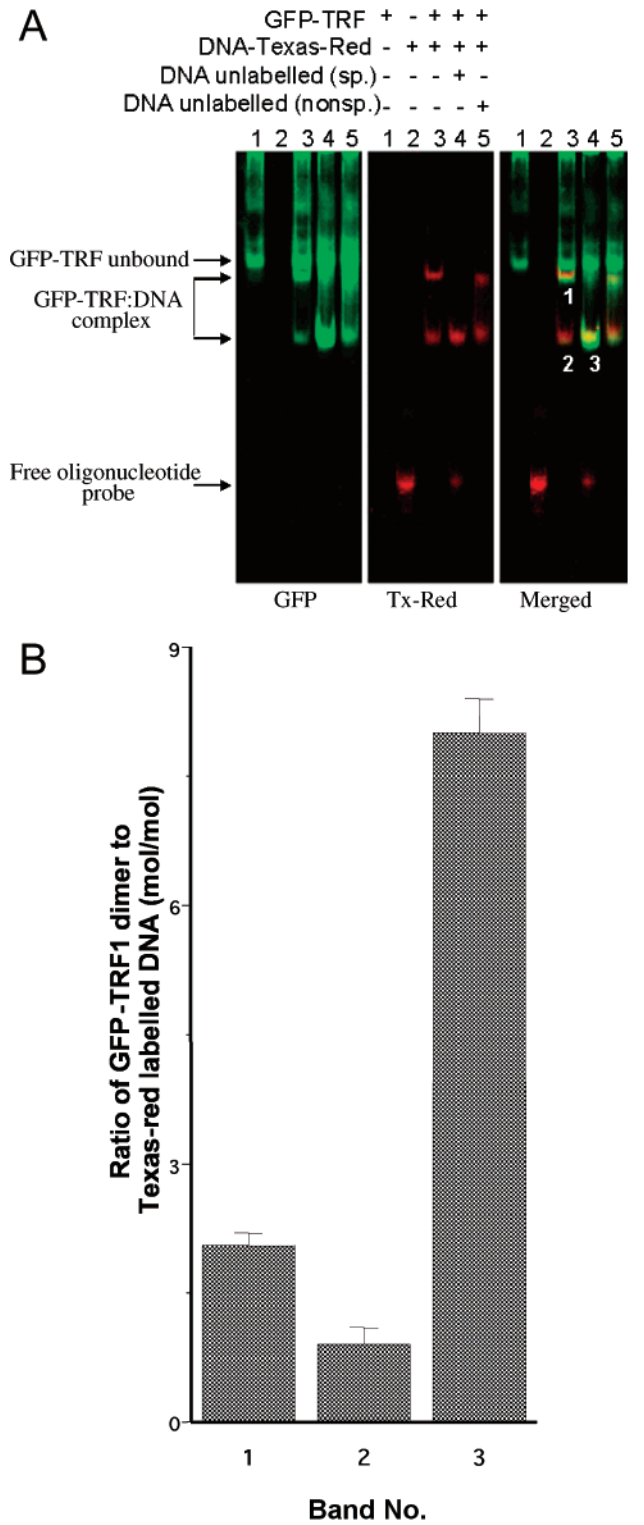

FIGURE 1: GFP−TRF1$_{337–441}$ is able to bind telomeric DNA as demonstrated by native gel electrophoresis. (A) Fluorescent gel image after electrophoresis of GFP−TRF1$_{337–441}$ in the absence (lane 1) or presence of annealed telomeric oligonucleotide labeled with Texas Red (lanes 3−5). The labeled oligonucleotide was incubated in the absence (lane 2) or presence of GFP−TRF1$_{337–441}$ (lanes 3−5) and in the absence (lanes 1−3) or presence of excess (10-fold) unlabeled probe containing either a specific (telomeric site for TRF1, lane 4) or an irrelevant binding site (see Materials and Methods, lane 5) as indicated. Green (GFP) and red (Texas Red DNA probe) fluorescence is shown in the left and middle panels, respectively, with the merged image on the right. (B) The molar ratio of the GFP−TRF1 dimer to Texas Red DNA for the bands numbered in (A) was determined using the ImageGauge software. After the subtraction of background values, the fluorescence associated with each band for GFP−TRF1 (green panels) or Texas Red DNA (red panels) was expressed as a percentage of the total protein/DNA present (40 pmol of dimer and 4 pmol, respectively) to enable the molar ratio to be determined. Results are for the mean ± SD for two separate experiments.

tions in solution (*11*, *17*, *19*, *20*). When plane-polarized light is used to excite a fluorophore, molecules whose absorption oscillators are orientated parallel to the direction of polarization are excited preferentially. The polarized components of the emission can be used to calculate an anisotropy ratiometric value $A = (I_{||} - I_{\perp})/(I_{||} + 2I_{\perp})$, which is dependent on the rotational mobility of the fluorophore, which in turn relates directly to its size, whereby larger fluorophores (with lower rotational mobility) exhibit higher anisotropy values under constant buffer conditions. Anisotropy measurements were used to analyze Imp binding to GFP/GFP−TRF1, where the concentration dependence of the changes in anisotropy, rather than the actual extent of the change, was used to estimate the affinity of the binding interaction. Measurements were carried out using the Polarstar 96-well fluorometer fitted with polarization filters. Excitation was at 485 nm, and light emitted from the fluorophore was collected after passage through a 520 nm cutoff filter. For each assay, GFP−TRF1 was diluted to a final concentration of 30 nM in PBS in the absence and presence of Imps (1−1000 nM). Results for changes in anisotropy were fitted to the equation $A = A_{max}x/(K_d + x)$, where x is the Imp concentration, A is the change in anisotropy, and the K_d is the Imp concentration giving half-maximal change in anisotropy.

RESULTS

We identified a putative NTS (KKKKESRR^{356}) homologous to that (PKKKRKV^{132}) of Simian virus SV40 large tumor antigen (T-ag) in the primary sequence of TRF1 N-terminal to the DNA-binding domain (TRF1 residues 378−439). To confirm that this region of TRF contains the NTS and to investigate the pathway by which it mediates nuclear translocation of TRF1, we generated a plasmid construct encoding a fusion protein (41 kDa), comprising hexahistidine-tagged GFP and TRF1 residues 337−441 including the NTS and DNA-binding domain, which is comparable in size to full-length TRF1 (*21*).

GFP−TRF1$_{337–441}$ Specifically Recognizes Telomeric DNA. The GFP−TRF1 fusion protein was expressed in bacteria and purified as described in Materials and Methods. To assess its functionality, a native gel mobility shift assay was performed using a DNA probe (see Materials and Methods) containing two telomeric binding sites (TTAGGG) in tandem which was labeled with Texas Red. As shown in Figure 1A, GFP−TRF1 reduced the migration of the probe (Tx-Red panel; compare lanes 2 and 3), indicative of binding. To ensure that the interaction was specific, we assessed the ability of excess nonlabeled probe to compete for binding. In the presence of a 10-fold excess of unlabeled probe, the labeled probe migrated at the unbound (free probe) position (Tx-Red panel; lane 4), implying that binding was specific. A 10-fold excess of unlabeled probe lacking telomeric DNA-binding sites did not compete for binding of the labeled probe (Tx-Red panel; lane 5), thus confirming that the interaction of GFP−TRF1 with the telomeric DNA probe was specific

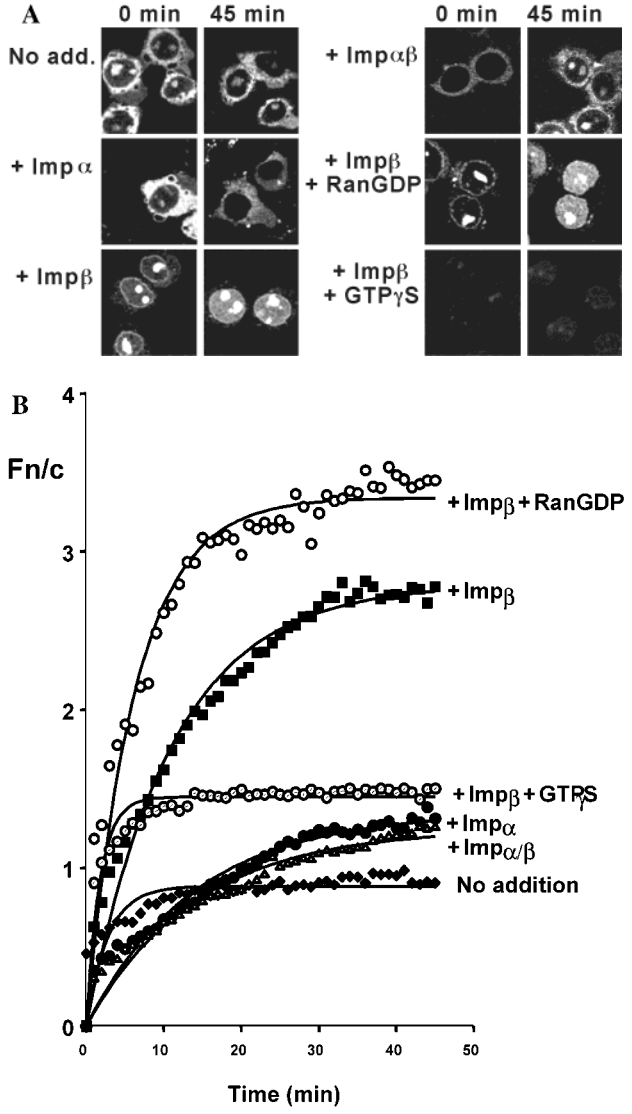

FIGURE 2: Nuclear import of GFP−TRF1$_{337-441}$ in vitro. Nuclear import of GFP−TRF1 was reconstituted using mechanically perforated HTC cells as described in Materials and Methods and followed for 45 min at room temperature in the absence or presence of Imps, RanGDP, or GTPγS as indicated. Real time movies representative of these experiments can be found at the URL http://www.med.monash.edu.au/biochem/research/projects/nuclearsig/realtimemoviesTRF1.html. (A) CLSM images after 0 and 45 min, as indicated. (B) Quantitative results for the nuclear import kinetics from a single typical experiment performed as per (A) for GFP−TRF1$_{337-441}$, where *F*n/c is the ratio of nuclear to cytoplasmic fluorescence. Data were fitted for the function $Fn/c = Fn/c_{max}(1 - e^{-kt})$, where Fn/c_{max} is the maximal level of nuclear accumulation, k is the rate constant, and t is time in minutes. Pooled data are presented in Table 1.

and that recombinant GFP−TRF1 is functional in DNA binding.

The use of dual fluorescent labels to track the migration of both DNA-binding proteins and DNA in native gels offers significant advantages over conventional native gel shift assays where only the position of the DNA in the gel can be directly monitored. The GFP tag on TRF1 permitted visualization of its running position, revealing for the first time that the protein−DNA complexes migrated with greater mobility than the DNA-binding protein alone (GFP−TRF panel; compare lanes 1 and 3), presumably as a result of the additional negative charge relative to protein alone. The ability to track the migration of the protein as well as DNA enabled determination of the makeup of the different DNA−protein bands. By quantitating the fluorescence intensity represented by the GFP−TRF1 and Texas Red DNA bands, subtracting background values, and converting into picomoles by measuring standardized amounts of the relative red and green chromophores in the same gel (see Materials and Methods), we were able to estimate the precise stoichiometry of protein to DNA in the different bands (Figure 1B). We determined that the upper (merged panel; band 1, lane 3) TRF1−DNA complex represents a 2.01 ± 0.15 ratio (mol/mol) of TRF1 dimer to DNA, ca. 2-fold that of the lower band (merged panel; band 2, lane 3), which exhibited a ratio of near 1 (0.9 ± 0.2). Consistent with the fact that TRF1 binds DNA as a homodimer (*4*) and that the DNA probe contains only two TTAGGG binding sites, it seems clear that the lower band represents a single TRF1 homodimer bound to DNA, while the upper band consists of two TRF1 homodimers bound to the two contiguous TTAGGG binding sites within the probe. In the presence of a 10-fold excess of unlabeled specific DNA (merged panel; band 3, lane 4), the TRF1−DNA complex ran predominantly as the faster migrating shifted band (see GFP panel), with a ratio of 8 ± 0.4, 9 times higher than the result in the absence of an excess of unlabeled DNA (merged panel; band 2, lane 3). This is consistent with the idea that this faster migrating band represents the 1:1 complex of TRF1 homodimer−Texas Red DNA probe, bearing in mind that only 1 in 11 of the DNA molecules running at this position in the case of the 10-fold excess of unlabeled telomeric probe can be visualized/quantitated. Essentially equal amounts of DNA are present within the two bands in the presence of limiting amounts of DNA (Tx-Red panel, lane 3), indicating that TRF1 exhibits negative cooperativity for the two telomeric repeats. This is also supported by lane 4 in the Tx-Red panel where, in the presence of excess DNA, the protein−DNA complex migrates predominantly almost exclusively as a single TRF1 homodimer−DNA complex, with almost no DNA fragments having two TRF1 homodimers bound. Since ca. 95% of the TRF−DNA complexes in lane 4 represent the single TRF1 homodimer−DNA complex, the estimated K_{coop} is less than 0.0001 (data not shown), underlining the strong negative cooperativity.

Table 1: Kinetics of Nuclear Import of GFP−TRF1 in Vitro

addition	nuclear transport parameters[a]		
	*F*n/c$_{max}$	$t_{1/2}$	*n*
none	0.8 ± 0.1	ND[b]	6
+Impα	1.1 ± 0.2	ND	4
+Impβ	2.8 ± 0.2	10.2 ± 1.5	6
+Impα/β	1.0 ± 0.1	ND	4
+Impβ + RanGDP	3.5 ± 0.3	4.6 ± 1.2	3
+Impβ + GTPγS	1.4 ± 0.1	ND	3

[a] Nuclear import kinetics were determined as described in Materials and Methods (see Figure 2 and movies thereof). Results represent the mean ± SEM (*n* indicated) for data fitted to the function $Fn/c = Fn/c_{max}(1 - e^{-kt})$, where *F*n/c$_{max}$ is the maximal level of nuclear accumulation and $t_{1/2}$ is the time in minutes taken to reach half-maximal accumulation (*12*−*16*). [b] ND, not able to be determined due to low accumulation.

TRF1$_{337-441}$ Mediates Nuclear Targeting through Direct Interaction with Impβ. To assess the nuclear translocation of TRF1, we used a well-characterized in vitro nuclear

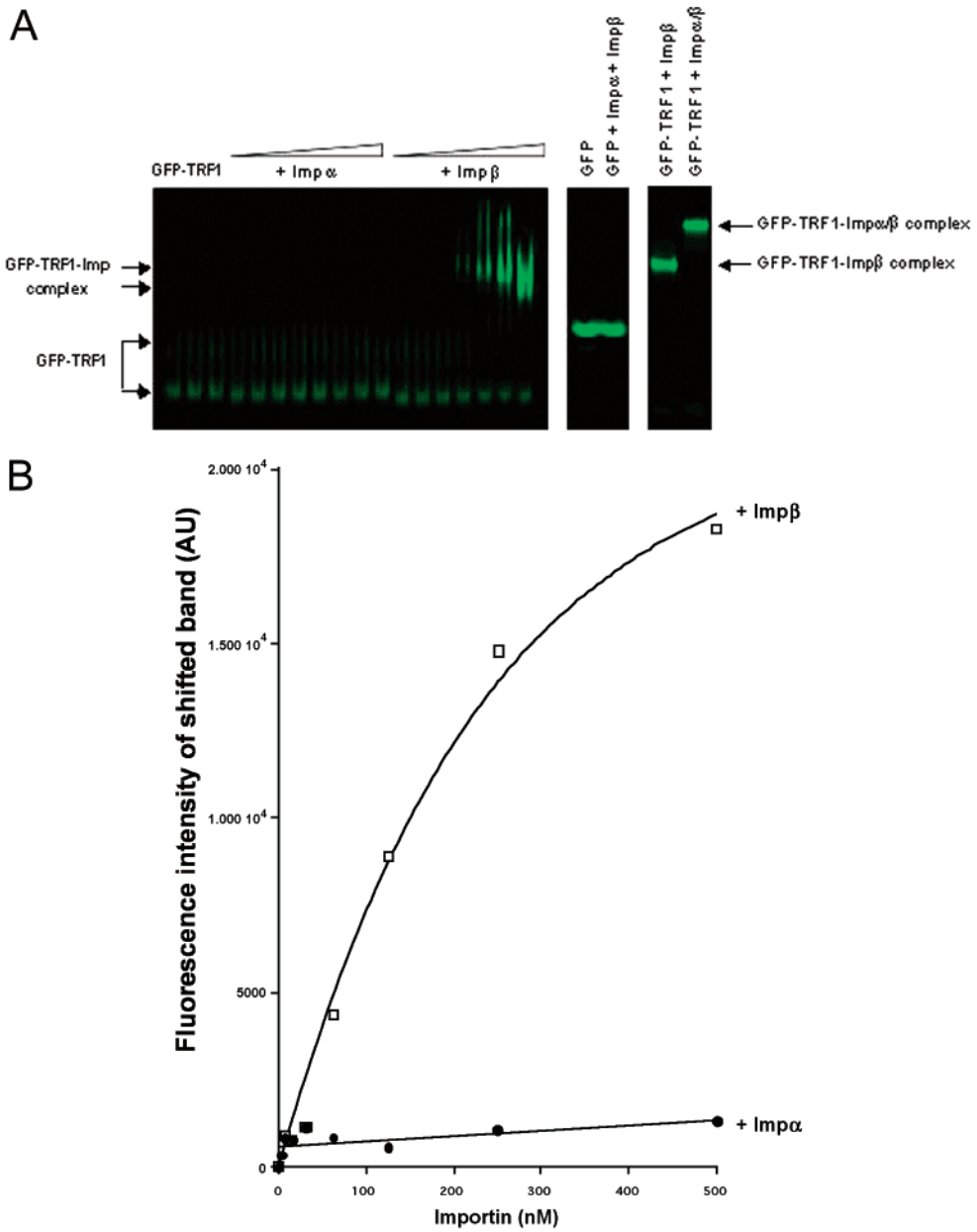

FIGURE 3: Impβ recognizes GFP−TRF1$_{337-441}$ with high affinity as shown by native gel electrophoresis. (A) Fluorescent image of a 5% native polyacrylamide gel after electrophoresis for 2 h at 30 mA. The position of GFP−TRF1$_{337-441}$ is shown in the absence (left panel, three left lanes) or presence of preincubation with the mouse Imp subunits indicated (25−3000 nM) prior to electrophoresis (left panel) and compared to GFP in the presence of 3000 nM importins (middle panel). The right panel shows a detail of TRF1 in the presence of Impβ or Impα/β (3000 nM). (B) Quantitation of fluorescence (ImageGauge software) from the left panel of (A), performed as described in Materials and Methods, with curves fitted to the function $A = A_{max}x/(K_d + x)$.

transport assay in conjunction with CLSM. We modified the assay to assess the nuclear transport of individual cells over a 45 min period, allowing nuclear import to be investigated in real time; movies representative of these experiments can be found at the URL http://www.med.monash.edu.au/biochem/research/projects/nuclearsig/realtimemoviesTRF1.html. We found that, in the absence of Imps or cytosolic factors, GFP−TRF1 did not localize in the nucleus, with a maximal nuclear/cytoplasmic fluorescence ratio (*F*n/c) of 0.8 (see Figure 2, Table 1). The presence of recombinantly expressed Impα did not enhance nuclear accumulation (*F*n/c_{max} of 1.1), but the addition of Impβ enabled GFP−TRF1 to accumulate in the nucleus to an *F*n/c_{max} value of almost 3 (Figure 2, Table 1). The time taken to reach half-maximal nuclear accumulation ($t_{1/2}$), was 10.2 min in the presence of Impβ. Interestingly, in the presence of preformed Impα/β heterodimer, the *F*n/c_{max} was only 1, indicating a lack of nuclear accumulation and implying that the Impα/β hetereodimer, in contrast to Impβ alone, is unable to mediate TRF1 nuclear import. When bound to Impβ, Impα thus appears to inhibit the latter's ability to transport TRF1 to the nucleus.

The fact that GFP−TRF1 appeared to accumulate in the nucleus in the presence of Impβ without a requirement for exogenously added Ran implied that residual Ran may be present in the nuclei of the permeabilized cells. The Ran dependence of TRF1 nuclear import was thus tested first by assessing whether the nonhydrolyzable GTP analogue GTPγS, which inhibits conventional Imp-dependent nuclear import by locking Ran in its GTP form in the cytoplasm, could inhibit Impβ-mediated nuclear import. GTPγS caused a

marked reduction in nuclear accumulation (Fn/c_{max} of 1.4; Figure 2, Table 1) compared to in its absence. We then assessed whether the addition of exogenous RanGDP could enhance Impβ-dependent nuclear accumulation. The Fn/c_{max} value of 3.5 indicated that this was indeed the case, with the nuclear import rate significantly increased by over 2-fold ($t_{1/2}$ of 4.6 min). The results clearly supported the role of Ran in TRF1 nuclear transport and thus confirmed that the TRF1 nuclear accumulation in the presence of Impβ alone (above) is likely to be due to residual Ran remaining after the perforation process; this is the basis of GTPγS-mediated inhibition of TRF1 transport.

Impβ Binds TRF1 in Native Gel Shift Assays. The observations from the in vitro nuclear transport assays clearly suggested that TRF1 is imported to the nucleus by Impβ. To test if GFP−TRF1 is recognized by Impβ directly, we performed a native gel mobility shift assay with GFP−TRF1 in the absence and presence of Imps. As shown in Figure 3A, Impα did not bind GFP−TRF1 (middle lanes of left panel), in contrast to Impβ which slowed the migration of GFP−TRF1, indicative of binding (right lanes of left panel). Interestingly, the precomplexed Impα/β heterodimer resulted in a "super-super shift" (Figure 3A, right panel), indicating that Impβ is able to bind GFP−TRF1 as a heterodimer with Impα. This indicates that Impα's ability to inhibit Impβ-mediated nuclear import (Figure 2) is not through preventing Impβ binding to TRF1 (see also Discussion). Binding of Imps to GFP alone was not observed (Figure 3A, middle panel), indicating the specificity of the results. By quantitation of the shifted bands within the gel (Figure 3B), the concentration of Impβ giving a half-maximal change in mobility could be calculated, with the K_d estimated to be 240 ± 30 nM.

High Affinity of the Impβ−TRF1 Interaction. To confirm the above results, fluorescence polarization (FP) assays were performed; this approach has been previously used to determine the binding affinities in solution between several different Imps for their transport substrates (*11*, *17*, *19*). Binding is indicated by a change in anisotropy with the degree proportional to the extent of the change in molecular weight of the fluorescent molecule resulting from complex formation/dissociation. The affinity of binding can be determined from the concentration that gives rise to a half-maximal change in anisotropy. Consistent with the native gel mobility shift assays, Impα bound with relatively low affinity (<1500 nM) while Impβ or the Impα/β heterodimer bound with around 160 ± 30 and 140 ± 25 nM, respectively (see Figure 4). As a control, GFP was used as a control where only nonspecific binding was observed (data not shown). The results thus support the findings from native gel electrophoresis that Impβ is able to bind GFP−TRF1 as a heterodimer with Impα and that Impα, therefore, does not mask the binding site on Impβ for TRF1.

The N-Terminus of Impβ Recognizes TRF1. To perform preliminary analysis to assess which region of Impβ was responsible for binding to TRF1, we tested full-length human Impβ1 (hImpβ) and fragments thereof (*11*, *17*) for their ability to bind to GFP−TRF1 in FP experiments. We found that full-length hImpβ bound TRF1 with affinity similar to that of the mouse Impβ (K_d of 179 ± 25 nM; Figure 5, left panel). Significantly, both C-terminally truncated forms of hImpβ, Impβ (1−643) and Impβ (1−380), also bound GFP−TRF1 with similar affinities (K_ds of 178 ± 11 and 135 ± 26 nM, respectively; Figure 5, left panel). Control experiments performed using GFP alone showed negligible binding (Figure 5, right panel), indicating the specificity of the results with respect to TRF1. The results thus indicate that the N-terminus of Impβ mediates binding to TRF1, which is in contrast to other Impβ-recognized DNA-binding proteins such as the cAMP response element binding protein CREB (*11*) and sex determining factor SRY (*17*), both of which require the Impβ C-terminus for binding. In additional FP experiments (not shown), we tested whether TRF1 could be recognized by the Impβ homologue RanBP5 (Impβ3) which, like Impβ, recognizes the β-Imp-binding (BIB) domain of the ribosomal protein rp23a (*18*). Only very weak binding was observed (K_d > 3000 nM), indicating that RanBP5 did not bind to TRF1 with high affinity and, accordingly, that the TRF1 NTS does not appear to resemble the BIB domain.

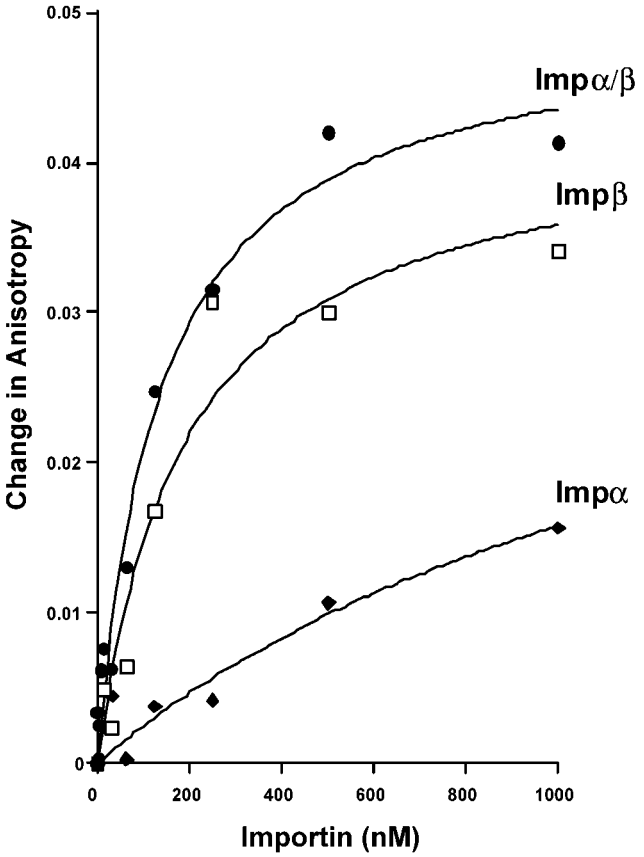

FIGURE 4: Impβ binds GFP−$TRF1_{337-441}$ with higher affinity than Impα as determined by FP. FP measurements for GFP−$TRF1_{337-441}$ in the presence of increasing concentrations of mImpα, mImpβ, and mImpα/β. Curves were fitted for the function $A = A_{max}x/(K_d + x)$, where x is the Imp concentration, A is the change in anisotropy (observed value minus initial value of 0.33), and the K_d is the Imp concentration giving a half-maximal change in anisotropy (*17*).

DISCUSSION

Telomere length is a dynamic process governed by the amount of TRF1 on the telomere and the activity of telomerase (*2*). While TRF1 has been shown in vivo to be bound to telomeres during interphase and metaphase (*5*), the mechanism by which it is transported to the nucleus had not been examined prior to this study. Here we use an established in vitro nuclear transport assay to monitor TRF1 nuclear accumulation in real time for the first time, in combination

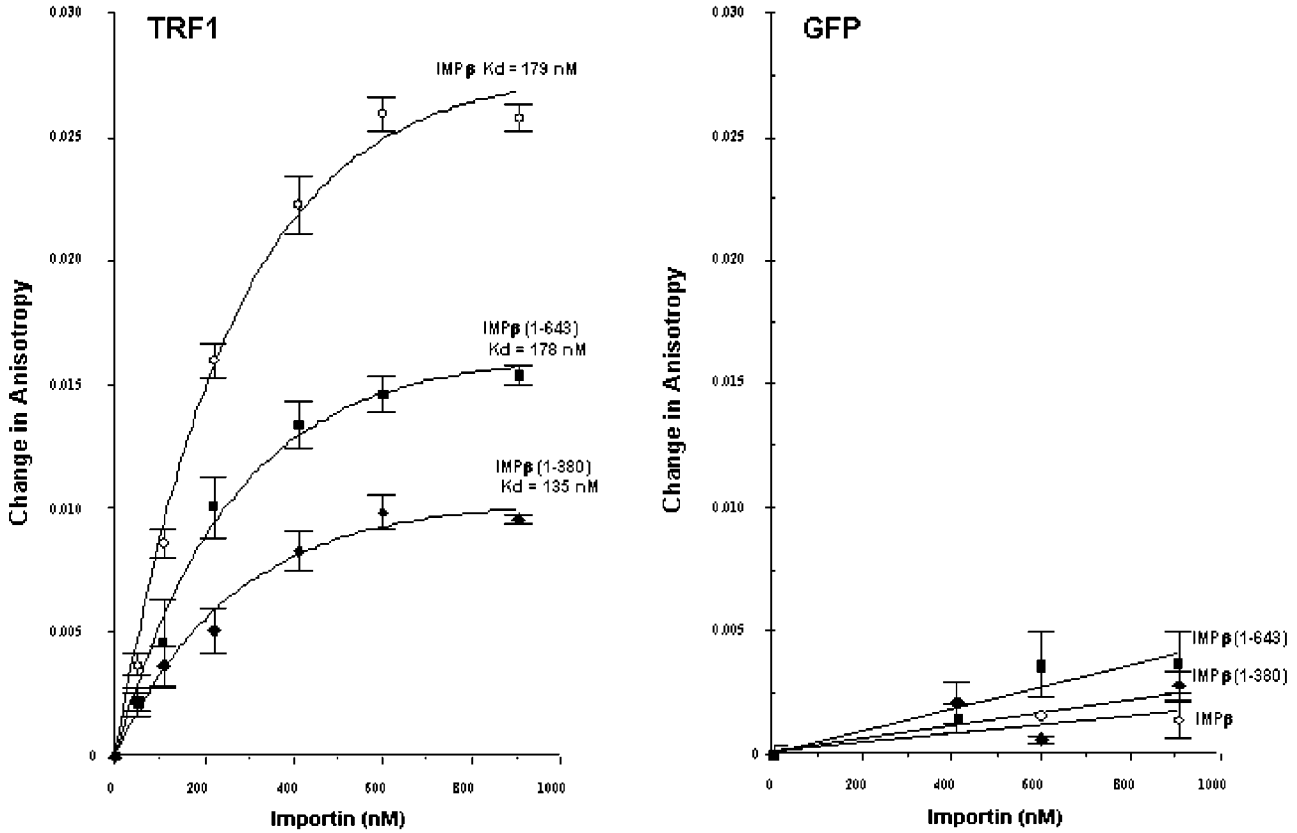

FIGURE 5: The N-terminus of Impβ mediates binding with TRF as determined by FP. FP measurements for GFP−TRF1$_{337-441}$ (left panel) and GFP alone (right panel) in the presence of increasing concentrations of the full-length and truncated forms of human Impβ as indicated. Curve fitting was performed as described in the legend to Figure 4, with the K_d calculated from the Imp concentration giving a half-maximal change in anisotropy; the latter is not influenced by the extent of the maximal change in anisotropy, which differs for the Impβ forms according to their molecular weight (see Materials and Methods and refs *11*, *17*, and *19*). The results represent the mean ± SD for two separate experiments (see also Results section).

with a range of binding assays. We demonstrate that TRF1 amino acid residues 337−441 are sufficient to target GFP to the nucleus (see Figure 2), through a nuclear import pathway dependent on Impβ and Ran. That DNA-binding domains may contain a functional NTS has been shown for a number of other TFs and DNA/RNA-binding proteins (*22*, *23*). Since nucleotide binding and NLSs are intrinsically basic sequences, it is presumed that the former may have evolved to perform both functions in primordial eukaryotes. The ability of these sequences to perform two distinct but related functions within a single or overlapping region of a protein may be advantageous in terms of reducing the number of functional domains and thereby energy requirements and also in minimizing the likelihood of the two functions being separated through mutation or alternate splicing (*23*).

This study shows that TRF1 nuclear import is mediated by Impβ1 rather than the conventional NTS receptor Impα/β. Interestingly, we also demonstrate that Impα inhibits nuclear accumulation of TRF1 mediated by Impβ. That Impα does not inhibit nuclear import by preventing Impβ binding to TRF1 was demonstrated in both FP and gel assays, where the affinity of Impβ for TRF1 was not reduced in the presence of Impα, and native gel mobility shift analyses, and a complex of TRF1 with the Impα/β heterodimer could be demonstrated. That an Impβ1-mediated nuclear import pathway can be inhibited by Impα has previously been shown for PTHrP (*24*) and GAL4 (*22*), while Görlich and co-workers (*18*, *25*) have reported recognition of nuclear import substrates such as ribosomal proteins rpL23a and histone HI by Impα/β which are "nonproductive" in terms of not leading to nuclear import (see also ref *10*). Impα recognition of prothymosin α also appears not to be sufficient for nuclear accumulation (*26*). Thus, high-affinity complexation of Imps with a potential nuclear import substrate does not necessarily lead to nuclear translocation but can in effect result in the inhibition of nuclear import. Significantly, Impα appears able to bind cytoplasmic cytoskeletal components such as microtubules (*27*−*29*; see also ref *30*), indicating a possible mechanism by which Impα/β may inhibit transport, conceivably through localizing the transport complex to cytoskeletal elements to effect cytoplasmic retention.

In the case of histone H1 (*25*), it has been shown that Impα binds Impβ at a site (the IBB domain) different from that recognizing histone H1; the transport properties of histone H1 are thus comparable to those for TRF1 here. That nuclear import of a chromatin component and a telomere binding protein can be negatively regulated by Impα/β is intriguing, opening up the possibility of a common pathway for the regulation of nuclear translocation of these types of DNA-binding proteins not directly involved in transcription (see ref *10*); histone H1 nuclear import is believed to require the Impβ homologue RanBP7 (Imp7) in a heterodimeric complex with Impβ1 and hence represents an import pathway quite distinct from that of TRF1. In this context, our results here indicate that residues 1−380 of Impβ are sufficient to mediate binding of TRF1, making it unlikely that the NTS

of TRF1 is analogous to the BIB domain of ribosomal protein rpL23a, which is able to be recognized independently by Impβ1, as well as Impβ2, RanBP5, and RanBP7 (*18*). Binding of Impβ to the rp23a BIB is known to be mediated by Impβ residues 286−462 (whereby Impβ 1−409 is unable to bind the BIB; *18*) so that it seems clear that the TRF1 NTS is not comparable to the BIB, while the fact that RanBP5 does not appear to recognize TRF1 (see Results section) is consistent with this. TRF1 would thus appear to possess a novel NTS that confers specific interaction with the Impβ1 N-terminus and thus be distinct from the NTSs in bZIP transcription factors such as CREB (*11*) and the HMG-box-containing chromatin remodeling factor SRY (*17*), both of which require the Impβ C-terminus for binding. PTHrP (*24*, *31*) would appear to bind to the central region of Impβ (residues 380−643; *31*), indicating that at least three distinct NTS binding sites reside within the 19 HEAT repeats of Impβ, thus enabling a whole range of different types of molecules to be recognized by it (see refs *10* and *32*).

In the whole cell context, there is a multitude of NTS-containing nuclear import substrates competing for limiting numbers of components of the nuclear import machinery and NTS receptors in particular (*10*), so that a key factor in determining which proteins are imported is the affinity of the binding interaction between the NTS-containing protein and its requisite Imp. Since the affinity of TRF1 for Impβ determined here using FP and native gel mobility shift analysis is in the nanomolar range, it is likely that TRF1 is able to compete relatively effectively for Impβ and thereby localize efficiently in the nucleus in the whole cell context, although the inhibitory role of Impα as indicated may be an important factor.

The ability to maintain telomere length through successive cell divisions relates strongly to cellular disfunctions such as cancer and apoptosis, but the possibility of regulation of telomere length through modulation of the nuclear import of TRF1 or other telomere regulatory factors has not been considered until now. The results here demonstrating that Impβ mediates TRF1 nuclear import while Impα can play an inhibitory role, implicating their role in modulating TRF1's nuclear activity, should not be underestimated. The fact that overexpressed TRF1 causes telomere shortening (through increased TRF1 nuclear location/activity—*2*), for example, may be attributable to the high levels of TRF1 titrating out Impα/β in the cell to overcome cytoplasmic retention and allow higher levels into the nucleus. Further study in this area should aid in understanding the molecular basis of disease processes arising from deregulated TRF1 nuclear activity.

ACKNOWLEDGMENT

We thank Titia de Lange and Daniela Rhodes for supplying the TRF1 cDNA, Dirk Goerlich for providing the RanBP5 expression construct, and Anna John and Lakshmi Wijeyewickrema for cell culture/protein expression.

REFERENCES

1. Smogorzewska, A., van Steensel, B., Bianchi, A., Oelmann, S., Schaefer, M. R., Schnapp, G., and de Lange, T. (2000) *Mol. Cell. Biol. 20*, 1659−1668.
2. van Steensel, B., and de Lange, T. (1997) *Nature 385*, 740−743.
3. Bilaud, T., Brun, C., Ancelin, K., Koering, C. E., Laroche, T., and Gilson, E. (1997) *Nat. Genet. 17*, 236−239.
4. Broccoli, D., Smogorzewska, A., Chong, L., and de Lange, T. (1997) *Nat. Genet. 17*, 231−235.
5. Chong, L., van Steensel, B., Broccoli, D., Erdjument-Bromage, H., Hanish, J., Tempst, P., and de Lange, T. (1995) *Science 270*, 1663−1667.
6. Bayliss, R., Littlewood, T., and Stewart, M. (2000) *Cell 102*, 99−108.
7. Englmeier, L., Olivo, J. C., and Mattaj, I. W. (1999) *Curr. Biol. 9*, 30−41.
8. Izaurralde, E., and Adam, S. (1998) *RNA 4*, 351−364.
9. Jans, D. A. (1995) *Biochem. J. 311*, 705−716.
10. Jans, D. A., Xiao, C. Y., and Lam, M. H. (2000) *BioEssays 22*, 532−544.
11. Forwood, J. K., Lam, M. H., and Jans, D. A. (2001) *Biochemistry 40*, 5208−5217.
12. Efthymiadis, A., Shao, H., Hubner, S., and Jans, D. A. (1997) *J. Biol. Chem. 272*, 22134−22139.
13. Hubner, S., Xiao, C. Y., and Jans, D. A. (1997) *J. Biol. Chem. 272*, 17191−17195.
14. Hubner, S., Smith, H. M. S., Hu, W., Chan, C. K., Rihs, H.-P., Paschal, B. M., Raikhel, N. V., and Jans, D. A. (1999) *J. Biol. Chem. 274*, 22610−22617.
15. Xiao, C. Y., Hubner, S., and Jans, D. A. (1997) *J. Biol. Chem. 272*, 22191−22198.
16. Hu, W., and Jans, D. A. (1999) *J. Biol. Chem. 274*, 15820−15827.
17. Forwood, J. K., Harley, V., and Jans, D. A. (2001) *J. Biol. Chem. 276*, 46575−46582.
18. Jaekel, S., and Görlich, D. (1998) *EMBO J. 17*, 4491−4502.
19. Fanara, P., Hodel, M. R., Corbett, A. H., and Hodel, A. E. (2000) *J. Biol. Chem. 275*, 21218−21223.
20. Weber, G. (1953) *Adv. Protein Chem. 8*, 415−419.
21. Zhong, Z., Shiue, L., Kaplan, S., and de Lange, T. (1992) *Mol. Cell. Biol. 12*, 4834−4843.
22. Chan, C. K., Hubner, S., Hu, W., and Jans, D. A. (1998) *Gene Ther. 5*, 1204−1212.
23. LaCasse, E. C., and Lefebvre, Y. A. (1995) *Nucleic Acids Res. 23*, 1647−1656.
24. Lam, M. H. C., Briggs, L. J., Hu, W., Martin, T. J., Gillespie, M. T., and Jans D. A. (1999) *J. Biol. Chem. 274*, 7391−7398.
25. Jakel, S., Albig, W., Kutay, U., Bischoff, F. R., Schwamborn, K., Doenecke, D., and Gorlich, D. (1999) *EMBO J. 18*, 2411−2423.
26. Shakulov, V. R., Vorogjev, I. A., Rubtsov, Y. P., Chichkova, N. V., and Vartapetian, A. B. (2000) *Biochem. Biophys. Res. Commun. 274*, 548−552.
27. Gruss, O. J., Carazo-Salas, R. E., Schatz, C. A., Guarguaglini, G., Kast, J., Wilm, M., Le Bot, N., Vernos, I., Karsenti, E., and Mattaj, I. W. (2001) *Cell 104*, 83−93.
28. Kahana, J. A., and Cleveland, D. W. (2001) *Science 291*, 1718−1719.
29. Smith, H. M., and Raikhel, N. V. (1998) *Plant Cell 10*, 1791−1799.
30. Percipalle, G., Butler, P. J. G., Finch, J. T., Jans, D. A., and Rhodes, D. (1999) *J. Mol. Biol. 292*, 263−273.
31. Lam, M. H. C., Hu, W., Xiao, C.-Y., Gillespie, M. T., and Jans, D. A. (2001) *Biochem. Biophys. Res. Commun. 282*, 629−634.
32. Gorlich D., and Kutay, U. (1999) *Annu. Rev. Cell Dev. Biol. 15*, 607−660.

BI025548S